Tellus (2005), 57A, 654–661
Printed in Singapore. All rights reserved

TELLUS

A study of non-local effects on the Budyko–Sellers infrared parametrization using atmospheric general circulation models

By PETER L. LANGEN[1]* and VLADIMIR A. ALEXEEV[2], [1]*Niels Bohr Institute, University of Copenhagen, Juliane Maries Vej 30, 2100 Copenhagen O, Denmark;* [2]*International Arctic Research Center, University of Alaska Fairbanks, 930 Koyukuk Dr., PO Box 757340, Fairbanks, AK 99775-7340, USA*

(Manuscript received 2 November 2004; in final form 31 January 2005)

ABSTRACT

We perform a series of simplified atmospheric GCM runs with fixed zonally symmetric spherical harmonic sea surface temperature (SST) perturbations to study the response of the outgoing long-wave radiation (OLR) to SST anomalies of different horizontal scales and structures. The classical linear relationship used in energy balance models between the OLR and the SST holds quite well at high latitudes. This is not the case in the tropics; even for large-scale perturbations, especially antisymmetric about the equator, the correlation is poor. This is explained by the fact that the structure of the Hadley cell controls most of the properties of the tropical atmosphere, causing a local relationship between the surface and the top of the atmosphere to break down. This conclusion is supported by our analyses of the relationship between OLR and SST in the wavenumber domain. For very large-scale SST perturbations (wavenumbers 0–2) the agreement is reasonable – the OLR response has most of the energy in the same wavenumber. For higher wavenumbers, however, the correlation deteriorates and the OLR response has significant energy in other harmonics.

1. Introduction

Energy balance climate models (EBMs) have been used with great success in idealized studies of climate stability and sensitivity (e.g. Budyko, 1969; Sellers, 1969; North, 1975b) and have provided us with a tool to recognize the potential richness of the solution structure of the climate system (North, 1990). After the initial introduction in their simple form, EBMs have been used more widely in two-dimensional versions (e.g. Robock, 1983) and as upper boundary conditions in a hierarchy of ocean modeling experiments (e.g. Nakamura et al., 1994; Marotzke and Stone, 1995; Lohmann et al., 1996). In this manner, EBMs are still used for both research and teaching purposes.

The principal strengths of EBMs are their low computational cost and their tractability to analytical solutions (North, 1975a), both features that rely on simple parametrizations of the energy fluxes in the climate system. One such parametrization is the commonly used linear relationship

$$F_{\mathrm{I}} = A + BT_{\mathrm{S}}, \tag{1}$$

between the outgoing long-wave radiation (OLR), F_{I}, and the sea surface temperature, T_{S}. This is an empirical relationship linking the top of the atmosphere OLR to the local temperature at the surface; in this paper, we focus on the non-local effects that the atmospheric circulation has on this relationship and on the problems they pose.

By neglecting variations in the fractional cloud coverage Budyko (1969) was first to employ eq. (1). Sellers (1969) used a more complicated form of the dependence, which, however, is linear to within 1% in the interesting range of temperatures (North, 1975a). The value of the parameter A is of rather little importance for the stability and sensitivity of a given climate model. In fact, A is often used to tune the temperature to match a certain target profile (e.g. Warren and Schneider, 1979). Conversely, the parameter B has major influence on the behavior of EBMs, and numerous studies have focused on determining the optimum value (e.g. Warren and Schneider, 1979; Graves et al., 1993). Despite the many efforts, there still exists quite a wide range of possible values: Marani (1999) sums up previous estimates to lie between about 1.5 and 2.3 W m^{-2} K^{-1}. The simple value of 2.0 W m^{-2} K^{-1} is often chosen when EBMs are used for qualitative rather than quantitative purposes.

One reason for the ambiguities in the determination of B is the inability of eq. (1) to deal sufficiently with the effects of tropical

*Corresponding author.
e-mail: plangen@gfy.ku.dk

convection. While the range of tropical temperature variations is rather limited, observations show large variations in OLR from one tropical region to another (Bess et al., 1989). Low values of OLR are seen in regions with high-level cloudiness and cold cloud tops associated with convective activity, while high values are found mainly over deserts characterized by subsidence and clear skies. Such a difference in regimes has led researchers to construct parametrizations for clear and cloudy skies separately, both in modeling studies (Thompson and Warren, 1982; Gutzler and Stone, 1986) and in observational studies (Graves et al., 1993; Raval et al., 1994). Thompson and Warren included the vertical mean relative humidity along with surface temperature as a predictor of OLR and devised a parametrization from curve fitting the output of a detailed radiative model. These predictors were observationally confirmed by Raval et al. to yield good results. They argue that the moisture field, which has large influence on the OLR, is most directly represented by the column-integrated precipitable water; however, because this field is so tightly coupled to the temperature field, use of relative humidity provides more independent information. In a GCM study, Gutzler and Stone conclude that inclusion of a measure of the atmospheric lapse rate as a co-predictor with surface temperature is useful when considering results from climate change experiments. Both relative humidity and lapse rate are influenced by the large-scale circulation (such as the Hadley cell) and thus provide information about the non-local conditions, which in the present paper will be argued to have dominant influence at low latitudes. This was also found by Allan et al. (1999), who explained the occurrence of low-latitude regions with OLR and surface temperature being anticorrelated in terms of seasonal shifts of the Hadley cell and interannual variations in the Walker circulation.

As will be done in the following, Short et al. (1984) worked in terms of spherical harmonics in their appraisal of eq. (1). Using 1 yr of Nimbus-6 data they performed a spherical harmonic expansion of the time-varying temperature and OLR fields. Variances and covariances calculated in terms of these expansions were concluded to be dominated by the largest space and time-scales. Higher-order contributions to the OLR variability, which are not nearly as pronounced in the temperature variability, were attributed largely to cloud variability in tropical convection regions. Equation (1) was found to hold quite well in mid to high latitudes and this explains its success in modeling even the seasonal cycle in EBMs; it works where it has to (i.e. in the large low heat capacity continental interiors at mid and high latitudes).

The error made when neglecting the very cold cloud tops in the linear relationship of eq. (1) is, by Short et al. (1984), argued to be countered by a similar error in the albedo (where the effect of the high tropical clouds is also neglected), such that the net effect is a reasonable representation. According to Pierrehumbert (2004), however, the atmosphere (humidity, vertical stratification, etc.) changes drastically in cold extremes such as Snowball Earth scenarios. This may cause a breakdown of the above fortuitous cancellation of errors and exemplifies the potential hazards of extending linear relationships tuned to present-day conditions into vastly different climate regimes. On the same note, Warren and Schneider (1979) speculate that the high value of $B \approx 3$ W m^{-2} K^{-1} found over Antarctica may imply that a glacial world is subject to stability conditions unlike those of today. As proposed by Short et al., it may also simply be due to a combination of high altitudes and low surface temperatures.

Due to the nature of the available observations, the present-day latitudinal variations and seasonal cycle are commonly used to determine parametrizations of the OLR (e.g. Short et al., 1984; Raval et al., 1994). However, by comparing their variable-cloud-top-temperature and fixed-cloud-top-altitude parametrizations of the OLR, Neeman et al. (1987) demonstrated that successfully reproducing the present-day seasonal cycle is not sufficient for climate change studies. The two parametrizations yield similar seasonal cycles but imply a factor of 2 different sensitivities to solar constant changes. Similarly, the improvement in the parametrization that Gutzler and Stone (1986) gained from inclusion of lapse rate as a co-predictor was present only in climate change scenarios, and not in present-day runs. We speculate that the reorganizations of the large-scale circulation that render the lapse rate useful as a predictor are not captured by present-day variations. The perturbations introduced in the present study consist of zonally symmetric spherical harmonics and thus span the zonally symmetric parts of both present-day climate variations and climate change scenarios.

In Section 2 we describe the experiments and the two different GCMs employed therein. The results are presented and discussed in Section 3, and a summary and conclusion are offered in Section 4.

2. Experimental configuration

Two different models have been used in the experiments: the Goddard Space Flight Center GEOS model and the National Center for Atmospheric Research CCM3. Both models are run with aquaplanet boundary conditions and without the seasonal cycle. Instead, 'modified equinox' conditions as described by Alexeev (2003) are employed. The GEOS model is run at $4^\circ \times 5^\circ$ horizontal resolution with 20 layers in the vertical and the clouds zeroed out in the radiation code (as described by Alexeev, 2003). The CCM3 (described by Kiehl et al., 1996) is run at T21 horizontal resolution with 18 levels in the vertical and the full physics package included. Our modifications to the standard distribution of the model are described by Langen and Alexeev (2004) with the extra modification here that we exclude all effects of sea ice, i.e. the surface albedo is uniform and fixed and subfreezing grid points are treated as open water. The solar constant and CO_2 concentration are set to 1367 W m^{-2} and 355 ppm, respectively.

Before the experiments were started, both models were run with 50 m mixed layer oceans, such that the sea surface temperatures (SSTs) were allowed to settle into equilibrium. The

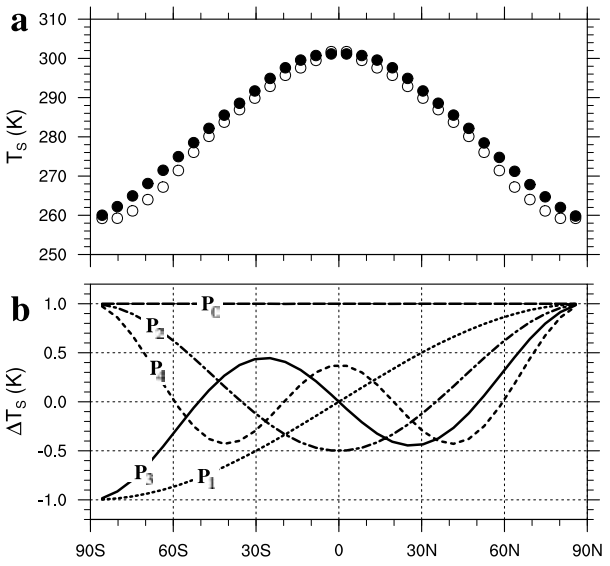

Fig. 1. (a) Reference SST profiles for the CCM3 (open circles) and the GEOS model (shaded circles). (b) The five first Legendre polynomial perturbations: long-dashed line, zeroth order; dotted line, first order; dash-dotted line, second order; solid line, third order; short-dashed line, fourth order.

surface albedo was tuned in both models to yield SST profiles similar to that of the present day. The models were then run for 20 yr in their respective equilibria and the SSTs were averaged over this period and symmetrized zonally and about the equator. The resulting SST profiles are termed the reference profiles and are plotted in Fig. 1a.

The actual experiment consists of a set of 17 fixed SST runs with both models: a reference run, where the temperature is fixed at the reference profile, and 16 perturbation runs, where the SST profiles are perturbed with the 16 first zonally symmetric spherical harmonics, i.e. zonally symmetric perturbations where the meridional structure is given by the 16 first Legendre polynomials in $\sin\phi$:

$$P_0(\phi) = 1, \quad P_1(\phi) = \sin\phi, \quad P_2(\phi) = \frac{1}{2}(3\sin^2\phi - 1), \quad \ldots.$$

The first five perturbations are illustrated in Fig. 1b. Note that the order of the polynomials corresponds to the number of roots, and that the parity of the order determines the symmetry of the polynomial. Even-ordered polynomials are symmetric about the equator, and odd ones antisymmetric.

While our truncated series naturally omits the smallest-scale features, the zonally symmetric spherical harmonics span all possible zonally symmetric perturbations. Apart from this mathematical property (which any basis possesses) the spherical harmonics are appealing because they are readily envisaged and can partially be related to physical processes and fields. The lowest even-order harmonics describe the typical large-scale patterns in climate change experiments, such as global warming and polar amplification. The first asymmetric harmonics describe both the seasonal cycle and possible hemispheric asymmetries in climate changes. Intermediate scales (of either parity) are needed when the effects of continents are to be addressed and the highest wavenumbers can be related to more localized features such as, for example, glaciers or oceanic upwelling areas.

All plots in the following are averaged zonally and over 20 yr of fixed SST perturbation runs.

3. Results

In Fig. 2 we have plotted the result of the first-order and second-order perturbation experiments. The solid lines show the temperature increases multiplied by 1.9 W m^{-2} K^{-1} and thus represent (the shape of) the changes in OLR one should see if eq. (1) holds. The value $B = 1.9$ W m^{-2} K^{-1} was chosen simply to facilitate the comparison, and actually agrees quite well with the optimum value of 1.93 W m^{-2} K^{-1} arrived at by Short et al. (1984). The dotted lines show the changes in all-sky OLR while the dashed lines show changes in clear-sky OLR, both for the CCM3 model. The former is the actual change while the latter is a diagnostic calculated internally in the code using the real temperature and moisture field but neglecting effects of clouds. The dash-dotted lines show OLR changes in the GEOS model, which has clouds zeroed out in the code, implying that the changes correspond most directly to the CCM3 clear-sky changes. In general, there is a fairly good correspondence between the actual and expected change in OLR. This is especially true at high latitudes in the clear-sky cases (dashed and dash-dotted lines), while with clouds

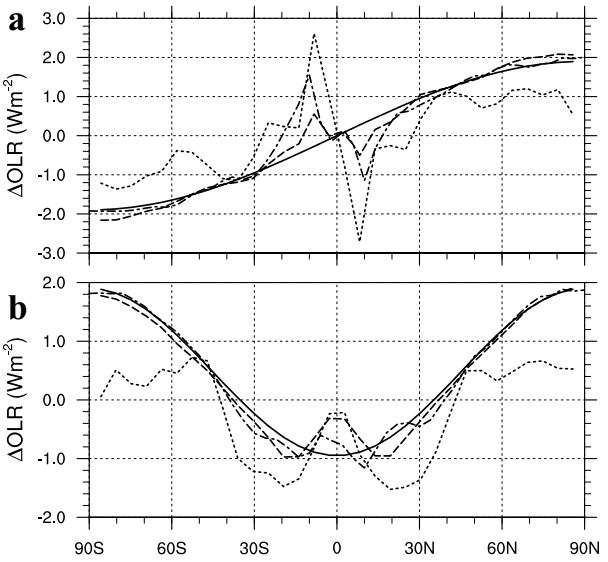

Fig. 2. OLR changes in the first-order (a) and second-order (b) perturbation experiments: solid line, SST change multiplied by 1.9 W m^{-2} K^{-1}; dashed line, CCM3 clear-sky; dotted line, CCM3 all-sky; dash-dotted line, GEOS model.

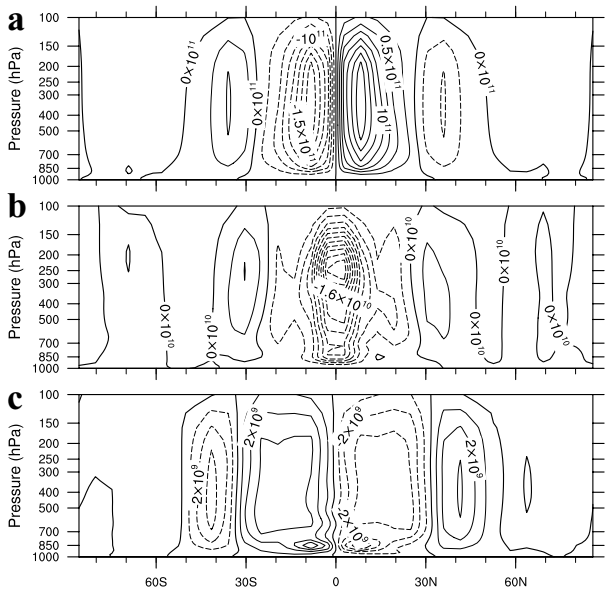

Fig. 3. Zonal mean meridional streamfunction (kg s^{-1}): (a) streamfunction in reference climate; (b) change when going to first-order perturbation; (c) change when going to second-order perturbation. All plots for CCM3 model.

there is generally an underestimation of the amplitude of the change poleward of ∼50°. This has to do with the very large cloud cover in the reference case (not shown), which, in fact, tends to shield the OLR change. Much of the OLR comes from the cloud tops such that when the surface temperature changes without the clouds changing significantly the OLR effect from the surface is damped.

In both the clear-sky and all-sky cases, the asymmetric perturbation yields a change in the OLR of the wrong sign in the off-equatorial region. In the symmetric case, this region shows an overestimation of the change while the equatorial region shows an underestimation of the change. These are features that clearly demonstrate the failure of eq. (1) in low latitudes. The problem is that a local relationship such as eq. (1) cannot adequately model the changes in dynamics that follow from the perturbations. Figure 3 demonstrates these changes in the CCM3. Figure 3a shows the zonally averaged meridional streamfunction in the reference case where the Hadley cells clearly stand out. Figures 3b and c show the changes in the streamfunction in the first- and second-order perturbations, respectively. The former is characterized by a large negative region centered over the equator; this is the footprint of a shift of the Intertropical Convergence Zone (ITCZ) – and the whole Hadley cell structure – into the Northern (warm) Hemisphere. Figure 3c shows a weakening of the circulation due to the decrease in meridional temperature gradient accompanying the perturbation. The importance of these changes for the OLR is due to the fact that the tropical moisture field is controlled mainly by the dynamics rather than the local temperature structure. Figure 4a shows the zonally averaged relative humidity field where the ascending branch of the tropical circulation is seen to be characterized by high values and the descending branch by low values. In Fig. 4b, which shows the changes associated with the asymmetric perturbation, we see a northward shift of the *RH* field, while in Fig. 4c, corresponding to the symmetric perturbation, a moistening of the descending branch and a drying of the ascending branch are seen. The small line-plots attached to the two-dimensional plots show the height-mean relative humidity

$$\widehat{RH} = \frac{1}{H}\int_0^H RH(z)\,\mathrm{d}z, \tag{2}$$

which, as mentioned in the introduction, was shown by Thompson and Warren (1982) and Raval et al. (1994) to be an effective co-predictor of OLR. The value of $H = 12$ km was found by Thompson and Warren to work well, and is employed here. Raval et al. put forth that the success of this definition of $\widehat{RH}$, rather than the more intuitive pressure-weighted average, may stem from its preferential weighting of the upper-tropospheric moisture field. The reference profile (Fig. 4a) of this number reiterates the influence of the circulation on the moisture field. The changes compare very well with the discrepancies in Fig. 2. In Fig. 2a, the downward spikes in the OLR in the Northern Hemisphere are positioned exactly in the same place as the upward (moist) spike in Fig. 4b, and vice versa for the Southern Hemisphere. In Fig. 2b, the overestimation of the off-equatorial OLR decrease coincides with the moistening seen in Fig. 4c due to the decreased strength of the Hadley cell. Likewise, the underestimation of the decrease over the equator coincides with the drying.

3.1. Determining the linear sensitivity parameter

A value of the sensitivity parameter, B, has been determined for each of the perturbation experiments by performing area-weighted linear regressions of the changes in OLR with the changes in SST. In the zero-order case, of course, the regression fails because all points have the same SST change, and here we have simply taken the area-weighted ratio of the OLR change to the SST change. For all perturbations, in both the clear-sky and all-sky cases, the above regression was performed using the whole globe, the tropics (30°S–30°N) and the extratropics (poleward of 30°S and 30°N), respectively. The result is shown in Fig. 5 where Fig. 5a displays the all-sky case, Fig. 5b the clear-sky case and Fig. 5c the results from the GEOS model. The solid lines are for the whole globe, the dashed lines are for the tropics and the dotted lines are for the extratropics.

In the all-sky case (Fig. 5a) we see large variations in the estimate for B, especially at low latitudes – a result that seems rather discouraging for the ability of EBMs to model the all-sky tropics. The high-latitude estimate is reasonable for large-scale perturbations, but as higher wavenumbers are approached the

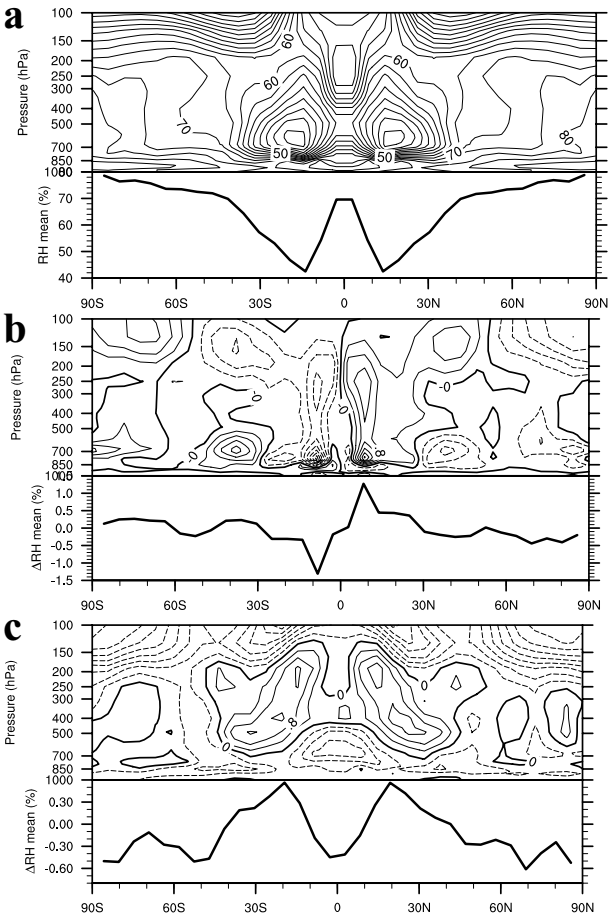

Fig. 4. Relative humidity (%): (a) reference climate with height-mean attached; (b) change when going to first-order perturbation; (c) change when going to second-order perturbation. All plots for CCM3 model.

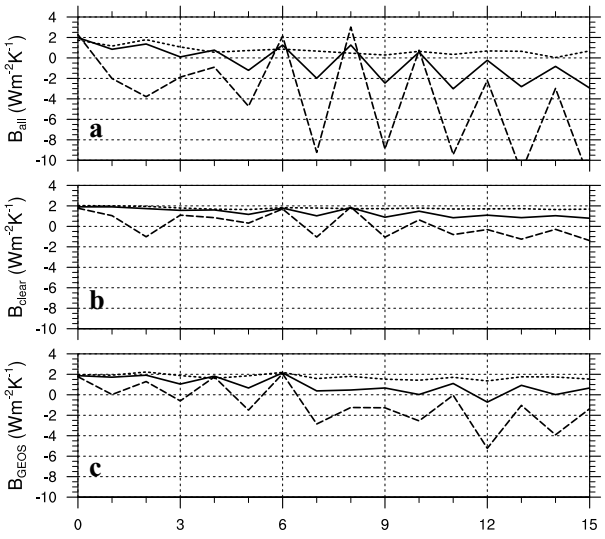

Fig. 5. Estimates of the sensitivity parameter, *B*. (a) CCM3 all-sky: solid line, based on whole globe; dashed line, tropics; dotted line, extratropics. (b), (c) As in (a) but for CCM3 clear-sky and GEOS models, respectively.

above-mentioned high-latitude cloud shielding effect tends to dominate and the sensitivity tends to zero. At higher wavenumbers, the asymmetric perturbations yield highly negative estimates for *B*. This is a consequence of the effect that was discussed above for the first asymmetric perturbation. The entire meridional circulation changes position and the resulting changes in the relative humidity field and especially the cloud field yield OLR changes with no connection to the local temperature change.

Considering still the CCM3, the high-latitude estimate of the sensitivity is rather consistent in the clear-sky case (Fig. 5b). It does not vary much with wavenumber and its value is close to the canonical value of $\sim$2 W m^{-2} K^{-1}. This is not the case at low latitudes where, at wavenumber 2, we already see that the large underestimation of the OLR change in the ITCZ (Fig. 2b) causes the slope of the regression line to become negative. It is important to stress that this negative value does not imply that a local rule holds in the tropics saying that the OLR decreases with increasing SST. It simply reflects the complete breakdown of any local relationship in the tropical region. Going towards higher wavenumbers, the odd-order perturbations tend to cause more problems for the low-latitude estimate than do the even-order perturbations. This seems to imply that when considering small-scale perturbations in the CCM3, the strength of the meridional circulation is less vulnerable than its position – the effect of shifting the Hadley cell is more pronounced than the effect of changing its strength. The global estimate of *B* remains positive throughout the range of wavenumbers, but, influenced by the tropical failure of the parametrization, the value tends away from 2 W m^{-2} K^{-1} at higher wavenumbers. An interesting exception is the value at wavenumbers 6 and 8 where all three regions (globe, tropics, and extratropics) yield almost perfect results. The reason for this is illustrated in Fig. 6 where results from wavenumbers 4, 8, and 12 are shown. As in Fig. 2, the solid lines are the temperature increases multiplied by 1.9 W m^{-2} K^{-1} and the dashed lines are the actual clear-sky OLR changes. The cartoon displayed by the three panels demonstrates how the intermediate wavenumber 8 (applies also to 6, not shown) matches the horizontal scale of the tropical circulation such that a change in the strength and the accompanying changes in the moisture field has the same meridional structure as the applied perturbation. At smaller and larger scales, the overturning strength changes without the resulting OLR changes resembling the perturbation.

In the GEOS model (Fig. 5c) the estimates look, as expected, more like the CCM3 clear-sky estimates than the all-sky estimates. The high-latitude value remains reasonably close to 2 W m^{-2} K^{-1} throughout the considered range of experiments. For large scales, the low-latitude estimate alternates between positive values for even perturbations and negative values for odd

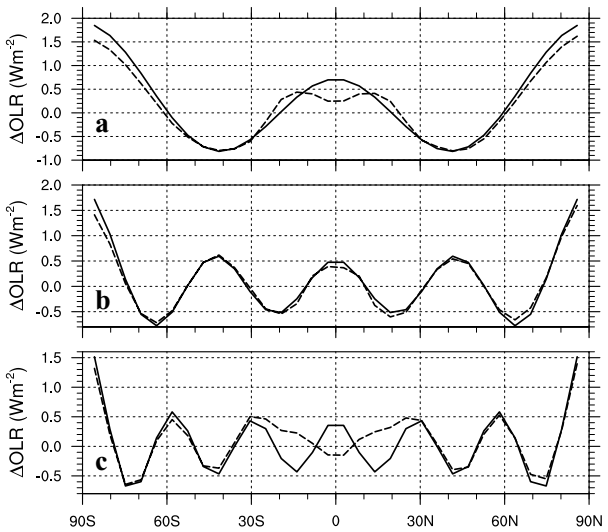

Fig. 6. As in Fig. 2 but for fourth-order (a), eighth-order (b) and twelfth-order (c) perturbations: solid line, SST change multiplied by 1.9 W m^{-2} K^{-1}; dashed line, CCM3 clear-sky.

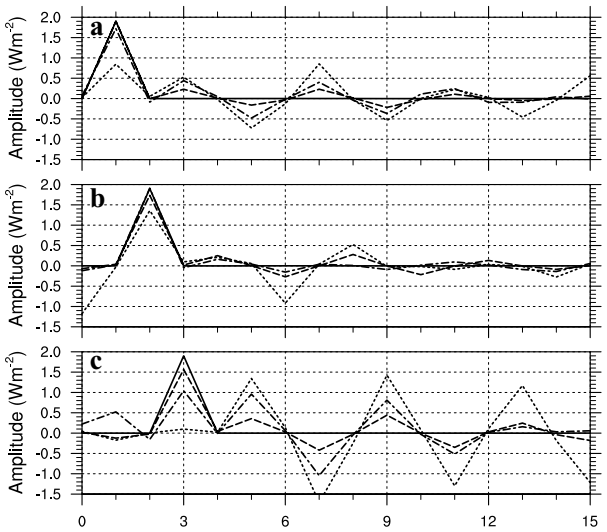

Fig. 7. As in Fig. 2 but in wavenumber space: (a) first-order, (b) second-order and (c) third-order perturbations.

perturbations, indicating again that shifting the Hadley cell has more impact on the OLR than changing its strength. At intermediate wavenumbers (4 and 6) we again see the low-latitude estimate being close to 2 W m^{-2} K^{-1}. As opposed to the clear-sky CCM3 case, where it was due to the perturbation having the same structure as the change in the circulation, the result is now simply a fortuitous cancellation of errors. Both structure and amplitude of the OLR change are quite different from the perturbation. At higher wavenumbers there is a reversal of the behavior with even orders giving more negative estimates than odd orders, such that for smaller-scale perturbations the strength change effect seems to dominate over the shifting effect. In neither case, however, does the low-latitude OLR change have any reasonable correspondence to the perturbation.

3.2. Results in wavenumber space

A different way of displaying our results is to make plots corresponding to Fig. 2 in the basis of Legendre polynomials. Figure 7 shows the results of the first-, second- and third-order perturbations. The solid lines are again the temperature increases multiplied by 1.9 W m^{-2} K^{-1} while the dashed lines and dotted lines are the changes in OLR for the CCM3 clear-sky and all-sky cases, respectively. The dash-dotted lines are the GEOS model OLR changes. In Fig. 7a, showing the first asymmetric perturbation, the dashed line falls quite closely on top of the solid line, reflecting the good match between the calculated change and the CCM3 clear-sky OLR change in Fig. 2a. The dash-dotted line (GEOS) reflects how the larger error in the tropics places more power on the higher wavenumbers. The dotted line (CCM3 all-sky) shows how the cloud shielding effect reduces the power in wavenumber 1 and how the shifts in the low-latitude cloud field place significant amounts of power on higher wavenumbers. A similar picture emerges in Fig. 7b (wavenumber 2) where the cloud shielding effect, however, works in the same direction in both hemispheres and places power on the zeroth wavenumber. The circulation changes associated with the large-scale symmetric perturbation lead to no significant error in the GEOS model and the dash-dotted line is even better than the dashed line corresponding to the CCM3 clear-sky case. In Fig. 7c the CCM3 all-sky OLR change is seen to have practically no resemblance with the temperature perturbation. There is no power on the perturbed wavenumber while it is distributed among all the higher odd-order wavenumbers. The CCM3 clear-sky and GEOS curves are more well behaved, although the fits have deteriorated as compared to the two previous perturbations.

The root-mean-square (rms) distance between the solid curve and the dashed, dotted, and dash-dotted curves, respectively, can be used as a measure of how well eq. (1) performs at a given wavenumber. In Fig. 8 we have plotted this difference for the CCM3 clear-sky (solid) and all-sky (dashed) cases and for the GEOS model (dotted) as a function of wavenumber. A feature common to all three cases is the deterioration of the relationship with decreasing horizontal scale. An exception to this is the good fit in the CCM3 at intermediate even wavenumbers where the horizontal structure of the perturbation, as mentioned, matches the changes induced in the circulation.

It is also apparent how the symmetric perturbations in general yield better results than the asymmetric perturbations, which, as we have seen, induce a shift in the position of the ITCZ. There are two exceptions to this. (i) In the CCM3 clear-sky case, the first asymmetric perturbation gives as good a fit as the two first symmetric perturbations. The changes in strength are, at the largest scales, as important as the shift of the circulation. As intermediate scales are approached, the asymmetric shifts in the ITCZ

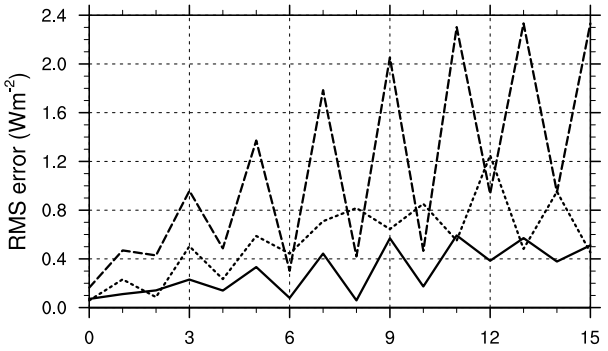

Fig. 8. The rms distance between actual and expected wavenumber space representations of OLR change: solid line, CCM3 clear-sky; dashed line, CCM3 all-sky; dotted line, GEOS model.

tend to decrease the projection of the OLR change onto the perturbation, giving worse fits, while the symmetric perturbations tend to give even better fits. At the smallest scales, the asymmetric fits no longer deteriorate, but the symmetric perturbations no longer match the circulation changes and the errors become nearly as large as those for the asymmetric perturbations. (ii) For the GEOS model, we see that at the smallest scales the asymmetric perturbations tend to give smaller errors than the symmetric perturbations. Here the changes in the strength of the circulation associated with the symmetric perturbations are relatively large, tending to reverse the sign of the OLR change and placing most of the power on the neighboring even-order wavenumbers.

4. Conclusions

In two different GCMs, we have performed a series of Legendre polynomial perturbations of the surface temperature and analyzed the response in the OLR. For clear skies, the OLR response follows rather closely a linear relationship as eq. (1) at high latitudes. Due to large high-latitude cloudiness in the CCM3 reference climate, the all-sky OLR response is damped, leading to a worse agreement with eq. (1) at high latitudes. At low latitudes, the higher moisture content of the atmosphere becomes important, as does the meridional circulation which, to large extent, sets the structure of the low-latitude moisture field. As discussed by, for example, Allan et al. (1999), the seasonal shifts in convective regimes lead to off-equatorial areas displaying negative correlations between SST and OLR. This is also observed in our study where the asymmetric perturbations yield a shift in the Hadley cell and associated shifts in the relative humidity field, which, in turn, lead to spikes in the OLR directed in the opposite direction of the local temperature change. Associated with symmetric perturbations is another effect on the meridional circulation, which is not captured by the seasonal cycle. Changes in the meridional temperature gradient lead to strengthening (or weakening) of the Hadley cell, which leads to moistening (drying) in the ascending branch and drying (moistening) in the descending branch. These moisture changes were also seen to have large impact on the OLR. An interesting effect was seen in the CCM3 where symmetric perturbations of intermediate wavenumbers (6 and 8) led to circulation changes of comparable meridional structures such that the OLR changes were very well represented by eq. (1).

The role of cloud radiative feedbacks in climate sensitivity and stability is still much debated, especially when it comes to tropical dynamics. In terms of the OLR parametrization, it has been proposed (e.g. Short et al., 1984; Graves et al., 1993) that due to the cancellation of the long-wave and short-wave effects of clouds (as mentioned in Section 1) we should be on safe ground if we ignore the clouds in the parametrizations of both fluxes. Thus, we have in this paper presented both all-sky and clear-sky results from the CCM3. A large part of the disagreement in the all-sky case is, as mentioned, due to the rather excessive cloudiness in the CCM3 reference climate. We speculate that, with a decreased reference cloudiness, the all-sky case would behave more like the clear-sky case, and thus, at least at mid and high latitudes, yield better agreement with eq. (1).

The CCM3 all-sky OLR is not very well represented by eq. (1) while its clear-sky OLR is reasonably represented (Fig. 8). The results for the GEOS model, which, in fact, is a clear-sky model, lie between these two. With large, symmetric perturbations the GEOS model and the CCM3 clear-sky results are equally good, but at intermediate and small scales the CCM3's clear-sky response is closer to the linear relationship. In general, large-scale, symmetric perturbations produce OLR responses better in accordance with eq. (1) than do small-scale, asymmetric perturbations. This seems to imply that the Budyko–Sellers parametrization is best suited for the simplest annually averaged EBM experiments and that discrepancies are more liable to occur in experiments including the seasonal cycle (asymmetries), two dimensions, and continents (smaller scales). However, a feature common to all perturbations is that they yield good clear-sky results at high latitudes where the focus of EBM studies (of, for example, the ice-albedo feedback) typically lies.

Had we included continents, seasons, and longitudinally varying perturbations, changes in strength and position of monsoonal and other circulations would have led to problems similar to those encountered in the simplified setup. However, according to Short et al. (1984), the asymmetric part of the fields only accounts for a small part of the variance in the annual mean, and we may expect the results of our zonally symmetric experiments to account for the dominant part of annual mean quantities in climate change experiments.

In conclusion, tropical circulation and dynamics are so important for even the clear-sky OLR that a local relation with SST is insufficient. One could, of course, include some representation of the moisture field, but one would then be left with the task of determining that in an EBM. The solution that we propose is to use the matrix that is obtained when combining the full set of 16 plots corresponding to the three shown in Fig. 7. The i'th

plot gives the OLR response in all wavenumbers arising from a temperature perturbation in the i'th wavenumber. The OLR field can thus be calculated as

$$\mathbf{F}'_{\mathrm{I}} = [\mathbf{B}_1|\mathbf{B}_2|\ldots|\mathbf{B}_i|\ldots|\mathbf{B}_N]\mathbf{T}'_{\mathrm{S}},$$

where the columns of the **B** matrix are the vectors represented by the plots in Fig. 7. $\mathbf{F}'_{\mathrm{I}}$ is the OLR perturbation and $\mathbf{T}'_{\mathrm{S}}$ is the SST perturbation, both given in the N-dimensional basis of Legendre polynomials. A requirement for this parametrization to hold is that the OLR response is linear with respect to the different combinations of the Legendre polynomial SST perturbations. We have not yet checked this systematically, but in all our preliminary runs it has, in fact, been the case. This is encouraging for the possibility of running EBMs in Legendre space (as has often been done; North, e.g. 1975a) and in this manner including the non-local effects seen in the present study while still using a linear and inexpensive parametrization.

5. Acknowledgments

This work was supported by IARC/NSF Cooperative Agreement 330360-66900 and the University of Copenhagen. Several points of the paper have been sharpened considerably due to the suggestions of our anonymous reviewers.

References

Alexeev, V. A. 2003. Sensitivity to CO_2 doubling of an atmospheric GCM coupled to an oceanic mixed layer: a linear analysis. *Climate Dyn.* **20**, 775–787.

Allan, R. P., Shine, K. P., Slingo, A. and Pamment, J. A. 1999. The dependence of clear-sky outgoing long-wave radiation on surface temperature and relative humidity. *Q. J. R. Meteorol. Soc.* **125**, 2103–2126.

Bess, T. D., Smith, G. L. and Charlock, T. P. 1989. A ten-year monthly data set of outgoing longwave radiation from nimbus-6 and nimbus-7 satellites. *Bull. Am. Meteorol. Soc.* **70**, 480–489.

Budyko, M. 1969. The effect of solar radiation variations on the climate of the Earth. *Tellus* **21**, 611–619.

Graves, C. E., Lee, W-H. and North, G. R. 1993. New parametrizations and sensitivities for simple climate models. *J. Geophys. Res.* **98**(D3), 5025–5036.

Gutzler, D. S. and Stone, P. H. 1986. Infrared flux parametrizations derived from climate changes in a three-dimensional climate model. *J. Geophys. Res.* **91**(D7), 7797–7802.

Kiehl, J. T., Hack, J. J., Bonan, G. B., Boville, B. A., Briegleb, B. P. and co-authors. 1996. Description of the NCAR Community Climate Model (CCM3). Technical Report TN-420, CGD, National Center for Atmospheric Research, Boulder, CO, USA.

Langen, P. L. and Alexeev, V. A. 2004. Multiple equilibria and asymmetric climates in the CCM3 coupled to an oceanic mixed layer with thermodynamic sea ice. *Geophys. Res. Lett.* **31** (doi:10.1029/2003GL019039).

Lohmann, G., Gerdes, R. and Chen, D. 1996. Sensitivity of the thermohaline circulation in coupled oceanic GCM–atmospheric EBM experiments. *Climate Dyn.* **12**, 403–416.

Marani, M. 1999. Parametrizations of global thermal emissions for simple climate models. *Climate Dyn.* **15**, 145–152.

Marotzke, J. and Stone, P. H. 1995. Atmospheric transports, the thermohaline circulation, and flux adjustments in a simple coupled model. *J. Phys. Oceanogr.* **25**, 1350–1364.

Nakamura, M., Stone, P. H. and Marotzke, J. 1994. Destabilization of the thermohaline circulation by atmospheric eddy transport. *J. Climate* **7**, 1870–1882.

Neeman, B. U., Joseph, J. H. and Ohring, G. 1987. The sensitivity of the outgoing longwave radiation to surface temperature: modeling the opacity feedback and experiments with a variable cloud-top temperature provision. *J. Atmos. Sci.* **44**, 2995–3006.

North, G. R. 1975a. Analytical solution to a simple climate model with diffusive heat transport. *J. Atmos. Sci.* **32**, 1301–1307.

North, G. R. 1975b. Theory of energy-balance climate models. *J. Atmos. Sci.* **32**, 2033–2043.

North, G. R. 1990. Multiple solutions in energy balance climate models. *Paleogeogr., Paleoclim., Paleoecol.* **82**, 225–235.

Pierrehumbert, R. T. 2004. High levels of atmospheric carbon dioxide necessary for the termination of global glaciation. *Nature* **429**, 646–649.

Raval, A., Oort, A. H. and Ramaswamy, V. 1994. Observed dependence of outgoing longwave radiation on sea surface temperature and moisture. *J. Climate* **7**, 807–821.

Robock, A. 1983. Ice and snow feedbacks and the latitudinal and seasonal distribution of climate sensitivity. *J. Atmos. Sci.* **40**, 986–997.

Sellers, W. D. 1969. A global climatic model based on the energy balance of the Earth-atmosphere system. *J. Appl. Meteorol.* **8**, 392–400.

Short, D. A., North, G. R., Bess, T. D. and Smith, G. L. 1984. Infrared parametrizations and simple climate models. *J. Climate Appl. Meteorol.* **23**, 1222–1233.

Thompson, S. L. and Warren, S. G. 1982. Paramterization of outgoing infrared radiation derived from detailed radiative calculations. *J. Atmos. Sci.* **39**, 2667–2680.

Warren, S. G. and Schneider, S. H. 1979. Seasonal simulation as a test for uncertainties in the parametrizations of a Budyko–Sellers zonal climate model. *J. Atmos. Sci* **36**, 1377–1391.